A Model for the Generation of Coastal Seiches by Deep-Sea Internal Waves*

DAVID C. CHAPMAN AND GRAHAM S. GIESE

Woods Hole Oceanographic Institution, Woods Hole, Massachusetts

(Manuscript received 28 September 1988, in final form 19 March 1990)

ABSTRACT

A dynamical mechanism for the generation of coastal seiches by deep-sea internal waves is investigated using a linear, two-layer coastal model in which internal waves from the deep ocean impinge upon a step-shelf bottom topography. For periodic incident waves, a pronounced peak in the shelf response occurs at each coastal seiche frequency. The maximum amplitude over the shelf is almost directly proportional to the degree of stratification, suggesting that seiche activity should vary with seasonal changes in the stratification.

Based on the periodic solutions, Fourier transforms are used to determine the response to one or more internal-wave pulses, and the results are qualitatively consistent with observations. For geometry and stratification which are representative of the Caribbean coast of Puerto Rico, reasonably realistic incident pulses preferentially excite the basic seiche frequency, and a rather small amplitude pulse (10 m) can easily generate currents at the shelf break of 8–10 cm s^{-1}. Further, as is typical of the observed seiches, the time history of the modeled motions over the shelf can be rather irregular, depending on the pulse shape and the time delay between pulses.

1. Introduction

Recently Giese et al. (1982), Giese and Hollander (1987) and Giese et al. (1990) have reported evidence that large-amplitude coastal seiches are forced by tide-generated internal waves which impinge upon the coastal topography from the deep sea. The scenario is as follows. Tidal currents flowing over a sill form groups of solitary waves, which propagate hundreds of kilometers across the open ocean toward the coast (e.g., Apel et al. 1985). Shortly after the solitary waves reach the coast, large-amplitude seiches are observed in coastal sea-level records. The amplitudes of the coastal seiches are highly correlated with the spring–neap tidal cycle, i.e. seiche activity has a fortnightly distribution with the largest seiches following spring tides.

Although the observational evidence is strong, what has been lacking is a dynamical mechanism for the baroclinic–barotropic coupling that transfers energy from internal solitary waves to coastal seiches. Such a process may seem unintuitive because energy is more typically transferred from barotropic flows to baroclinic flows (e.g. the generation of internal tides). We propose here a simple model that demonstrates that the reverse energy transfer (baroclinic to barotropic) can be sufficient to account for the observed coastal seiches. The model (described in section 2) is a slightly modified version of the linear, two-layer model used by Chapman (1984) in which deep-sea internal waves are incident upon a step-shelf bottom topography. The assumption of linearity precludes a proper treatment of internal solitary waves, per se, so we do not attempt to study their propagation over large distances. Instead, we consider only the short time during which the waves interact with the topography—a time too short to obtain appreciable nonlinear or dispersive effects. In this situation, the general results for periodic forcing (section 3) can be used to study the shelf response to one or more linear, deep-sea, internal wave pulses (section 4) which then provides insight into the response to solitary-wave forcing. The strengths and weaknesses of this approach are elaborated in section 5 followed by some concluding remarks in section 6.

2. Model formulation

We consider a simple model (Fig. 1) in which the deep ocean (with depth H) is stably stratified with two immiscible fluids having slightly different densities. The upper layer has mean thickness h_1 and density ρ, while the lower layer has thickness $h_2 = H - h_1$ and density $\rho(1 + \epsilon)$, where $\epsilon \ll 1$. The deep ocean borders a step shelf with width L, constant depth d and a homogeneous fluid of density ρ. Thus, the interface depth h_1 is always greater than the shelf depth d. Rotation effects are neglected and motions are assumed linear. The problem consists of determining the response of the model to an internal gravity wave (on the interface ζ) incident from the deep ocean ($x = \infty$).

* Woods Hole Oceanographic Contribution Number 6927.

Corresponding author address: Dr. David C. Chapman, Woods Hole Oceanographic Institution, Woods Hole, Massachusetts 02543.

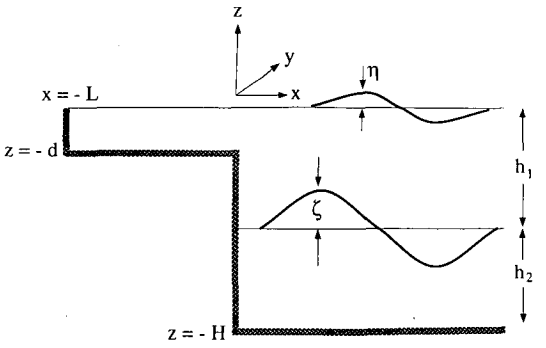

FIG. 1. Step-shelf topography with two-layer stratification in the deep sea.

After making the shallow-water (hydrostatic) approximation (justified in the Appendix), the equations of motion for this nonrotating, two-layer model are

$$u_t^U = -g\eta_x \tag{1a}$$

$$v_t^U = -g\eta_y \tag{1b}$$

$$(u_x^U + v_y^U)h_1 + \eta_t - \zeta_t = 0 \tag{1c}$$

$$u_t^L = -g[(1-\epsilon)\eta_x + \epsilon\zeta_x] \tag{2a}$$

$$v_t^L = -g[(1-\epsilon)\eta_y + \epsilon\zeta_y] \tag{2b}$$

$$(u_x^L + v_y^L)h_2 + \zeta_t = 0 \tag{2c}$$

where η and ζ are, respectively, the sea surface and interface displacements from rest; (u^U, v^U) and (u^L, v^L) are the cross-shelf (x) and alongshelf (y) velocities in the upper and lower layers, respectively; and g is gravitational acceleration. Subscripts x, y, t denote partial differentiation. Motions over the shelf are described by (1) with $\zeta = 0$ and h_1 replaced by d in (1c).

For simplicity, variables are scaled as follows:

$$x, y \text{ by } L$$

$$d, h_1, h_2 \text{ by } H$$

$$\eta, \zeta \text{ by } \zeta_i$$

$$u^U, v^U, u^L, v^L \text{ by } (g/H)^{1/2}\zeta_i$$

$$t \text{ by } L/(gH)^{1/2}$$

where ζ_i is the amplitude of the incident deep-sea internal wave. This scaling places the coast at $x = -1$, the shelf break at $x = 0$ and the deep-sea bottom at $z = -1$. Motions are also assumed monochromatic and propagating in the alongshelf direction with frequency ω and wavenumber l, i.e., $\propto \exp(i\omega t \pm ily)$ which allows oblique incidence of the internal wave.

Having specified an incident internal wave, solutions are obtained by first finding appropriate solutions for the shelf and for the deep-ocean regions separately, and then requiring continuity of surface displacement and cross-shelf mass transport at the shelf break ($x = 0$). Deep-ocean solutions are found by combining (1) and (2) into a single equation for the deep-ocean surface displacement (in scaled form),

$$\left(\frac{\partial^2}{\partial x^2} + \beta_+^2\right)\left(\frac{\partial^2}{\partial x^2} + \beta_-^2\right)\eta^D = 0 \tag{3}$$

where

$$\beta_+^2 = \left(\frac{\omega^2}{c_+^2} - l^2\right), \quad \beta_-^2 = \left(\frac{\omega^2}{c_-^2} - l^2\right),$$

$$c_\pm^2 = \frac{1}{2} \pm \frac{1}{2}(1 - 4\epsilon h_1 h_2)^{1/2}.$$

An appropriate solution of (3) is

$$\eta^D = Ie^{i\beta_- x} + Be^{-i\beta_- x} + Ce^{-i\beta_+ x} \tag{4}$$

where the unknown (complex) coefficients (I, B, C) represent the contributions to the surface displacement due to the incident internal wave, the reflected internal wave and the reflected surface wave, respectively. Note that (3) and (4) are written such that $lc_\pm < \omega$ results in real β_+, β_-; i.e. all waves are periodic in the cross-shelf direction.

Shelf solutions are found by combining the appropriate form of (1) into a single equation for the surface displacement which is (in scaled form)

$$\left(\frac{\partial^2}{\partial x^2} + \dot{\alpha}^2\right)\eta^S = 0 \tag{5}$$

where $\alpha^2 = (\omega^2/d - l^2)$. The solution of (5) which satisfies the boundary condition of no flow through the coast ($u = 0$ at $x = -1$) is

$$\eta^S = A\cos[\alpha(x+1)] \tag{6}$$

with unknown (complex) amplitude A.

The incident wave amplitude I is specified to correspond to the surface expression of an incident internal wave with unit (nondimensional) amplitude; that is

$$I = \mu^{-1} = (1 - h_1/c_-^2)^{-1}. \tag{7}$$

Using this value of I [an $O(\epsilon)$ quantity], the total surface displacement over the shelf or deep ocean represents the response due to an incident internal gravity wave with unit interface displacement. The dimensional η, ζ are recovered by multiplying the nondimensional values by ζ_i. The dimensional velocities are recovered by multiplying the nondimensional values by $(g/H)^{1/2}\zeta_i$.

The unknown amplitudes A, B, C are determined by requiring (i) continuity of surface displacement, (ii) continuity of upper-layer cross-shelf mass transport, and (iii) vanishing of the cross-shelf velocity in the lower layer of the deep ocean ($u^L = 0$), all at $x = 0$. This leads to three matching conditions at $x = 0$:

$$\eta^S = \eta^D \tag{8a}$$

$$d\eta_x^S = h_1\eta_x^D \tag{8b}$$

$$\eta_{xxx}^{D} + \left(\frac{\omega^2}{\epsilon h_1} - l^2\right)\eta_x^{D} = 0. \qquad (8c)$$

Substitution of (4), (6) and (7) into (8) produces three linear equations for the three unknown amplitudes A, B, C, the solution of which yields

$$A = 2\mu^{-1}/(\cos\alpha + \lambda i \sin\alpha) \qquad (9a)$$

$$B = A\cos\alpha - C - \mu^{-1} \qquad (9b)$$

$$C = \frac{-A\left(\dfrac{d\alpha}{h_1\beta_+}\right) i \sin\alpha}{\left[1 - \left(\dfrac{c_-^2}{c_+^2}\right)\left(\dfrac{\epsilon h_1 - c_+^2}{\epsilon h_1 - c_-^2}\right)\right]} \qquad (9c)$$

where

$$\lambda = \frac{\left(\dfrac{d\alpha}{h_1\beta_+}\right)\left[1 - \dfrac{\beta_+}{\beta_-}\left(\dfrac{c_-^2}{c_+^2}\right)\left(\dfrac{\epsilon h_1 - c_+^2}{\epsilon h_1 - c_-^2}\right)\right]}{\left[1 - \left(\dfrac{c_-^2}{c_+^2}\right)\left(\dfrac{\epsilon h_1 - c_+^2}{\epsilon h_1 - c_-^2}\right)\right]}$$

Equations (9) may be evaluated for any choice of the five parameters (ϵ, h_1, ω, l, d) provided that α, β_+, β_- are real and $d < h_1$.

3. Response to periodic forcing

We are most interested in the response over the shelf, so the discussion will concentrate on the shelf response A. Further, the parameters will typically be chosen to represent the shelf on the southwestern coast of Puerto Rico: shelf depth $\approx$ 18 m, shelf width $\approx$ 10 km, and deep-sea depth $\approx$ 4000 m (see Giese et al. 1990). The stratification varies seasonally, typically ranging from ϵ = 0.002 to 0.005 (e.g., Froelich et al. 1978). The upper-layer depth is assumed to be 128 m, which gives the same phase speed (for ϵ = 0.004) as that computed by Giese et al. (1990) for the lowest mode internal wave. The corresponding nondimensional variables are d = 0.0045 and h_1 = 0.032.

Choosing ϵ = 0.004, we have evaluated (9) for many combinations of incident frequency ω and alongshelf wavenumber l. The magnitude of the shelf response $|A|$ is shown in Fig. 2. The thicker diagonal line represents the boundary between periodic deep-sea surface waves (left) and offshore exponentially decaying deep-sea surface waves (right). Edge waves occur to the right of this line and were the subject of study by Chapman (1984). Within the periodic region, the response is nearly independent of l suggesting that the angle of incidence of the internal wave [given by $\tan^{-1}(l/\beta_-)$] is relatively unimportant. The largest response occurs along fairly narrow ridges which, not surprisingly, correspond to the barotropic coastal seiches which occur (for l = 0) at $\omega = d^{1/2}\pi(1/2 + n)$ for n = 0, 1, 2 · · ·. These peak responses are shown more clearly in Fig. 3 which is a slice through Fig. 2 along the frequency axis (l = 0). The peaks are not infinite, even without any frictional dissipation, because the seiches constantly leak energy offshore in the form of surface and internal gravity waves [last two terms on the right in (4)]. The maximum response (near resonance) is an order of magnitude greater than the background response (off resonance, e.g. $\omega \approx 0.2$), which becomes a difference of two orders of magnitude when considering energy.

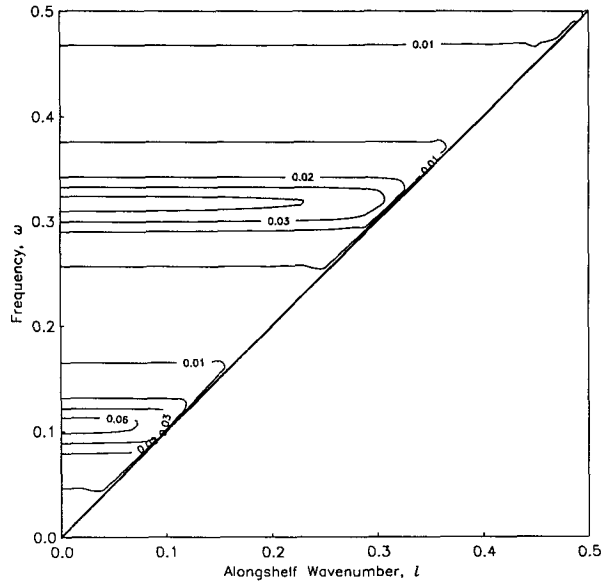

FIG. 2. Contours of the magnitude of the shelf response $|A|$ for various frequencies ω and alongshelf wavenumbers l. Other parameters are d = 0.0045, h_1 = 0.032, ϵ = 0.004. Coastal seiches are found only to the left of the thick diagonal line. Contour values are 0.01, 0.02, 0.03, 0.06.

An analytical expression can be found for the magnitude of the peak response from (9a) with l = 0 and $\epsilon \ll 1$:

$$|A|_{\max} = \frac{2\epsilon h_2}{d^{1/2}(1 + \epsilon^{1/2} h_2^{3/2} h_1^{-1/2})}. \qquad (10)$$

The maximum response is inversely proportional to the square root of the nondimensional shelf depth indicating that large coastal seiches forced by internal waves are more likely to be found over shallow shelves which border deep ocean basins. Also, the maximum response is almost linearly related to the stratification which suggests that the seiche activity should vary with the seasonal changes in stratification. The parameter dependence is shown in Fig. 4 where contours of $|A|_{\max}$ are plotted for various (ϵ, h_1) pairs. The strong dependence on ϵ is clear, while the dependence on h_1 is fairly weak near the value appropriate to Puerto Rico (h_1 = 0.032).

To put the values of $|A|_{\max}$ into perspective, if the incident internal wave has an amplitude of ζ_i = 10 m

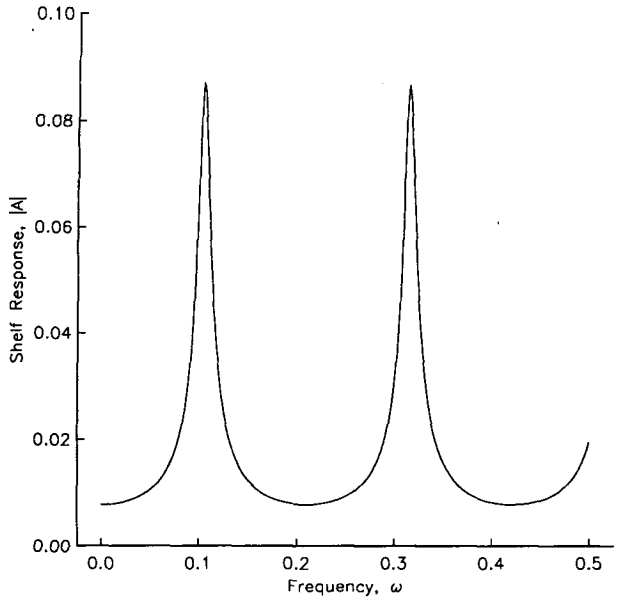

FIG. 3. Magnitude of the shelf response $|A|$ versus frequency ω for a normally incident internal wave ($l = 0$). Other parameters are $d = 0.0045$, $h_1 = 0.032$, $\epsilon = 0.004$.

(not large for this site; see Giese et al. 1990), then the lowest-mode seiche peak in Fig. 3 occurs at a period of 50 min and corresponds to a sea-surface displacement at the coast of 86 cm with a cross-shelf velocity at the shelf break of 64 cm s^{-1}, both very large values indeed!

4. Response to pulse forcing

The response described above is clearly supportive of the possibility that deep-sea internal waves could force large-amplitude coastal seiches. However, the periodic predictions for sea-level oscillations and currents at the shelf break are enormous. This results from the unrealistic assumption of a continuous train of incident waves at just the proper resonant frequency. Real internal waves do not typically occur in this form. In fact, tidally generated internal waves are expected to be more like a group of internal solitary waves (e.g. Apel et al. 1985). Giese et al. (1990) suggest that internal-wave packets may be generated in the southeastern Caribbean, and these would most likely be the forcing mechanism of interest for the present model study.

As mentioned above, the linearity of the present model precludes a proper treatment of solitary waves, which depend on some nonlinearity to remain intact. On the other hand, we can use the periodic results to investigate the response of the present model to a single event, or pulse, on the interface impinging upon the shelf. This approximates the response to a solitary wave as it gets close to the shelf break because the interaction time is too short for the nonlinear effects to be appreciable. The linear pulse maintains its structure because the shallow-water approximation renders the waves nondispersive (i.e. all of the individual components have the same phase speed). A group of pulses can be simulated in a similar manner.

Formally, the shelf response to a pulse traveling along the interface can be obtained using the Fourier transform in time and its inverse transform, defined by

$$\hat{G}(\omega) = \int_{-\infty}^{\infty} G(t)e^{-i\omega t}dt;$$

$$G(t) = \frac{1}{2\pi}\int_{-\infty}^{\infty} \hat{G}(\omega)e^{i\omega t}d\omega. \qquad (11)$$

The pulse is assumed to be normally incident upon the shelf ($l = 0$) with speed c_- and arbitrary shape, $\zeta^P(t + x/c_-)$. From the periodic results and (11), the sea surface and velocity over the shelf can be written as

$$\eta^S(x, t) = \frac{1}{2\pi}\int_{-\infty}^{\infty} \hat{\zeta}^P(\omega)A(\omega) \times \cos[\omega(x + 1)/\sqrt{d}]e^{i\omega t}d\omega \quad (12a)$$

$$u^S(x, t) = \frac{1}{2\pi i\sqrt{d}}\int_{-\infty}^{\infty} \hat{\zeta}^P(\omega)A(\omega) \times \sin[\omega(x + 1)/\sqrt{d}]e^{i\omega t}d\omega \quad (12b)$$

where the scaled form of (1a) has been used and $\hat{\zeta}^P(\omega)$ is the Fourier transform of ζ^P.

With the assumption of normal incidence ($l = 0$),

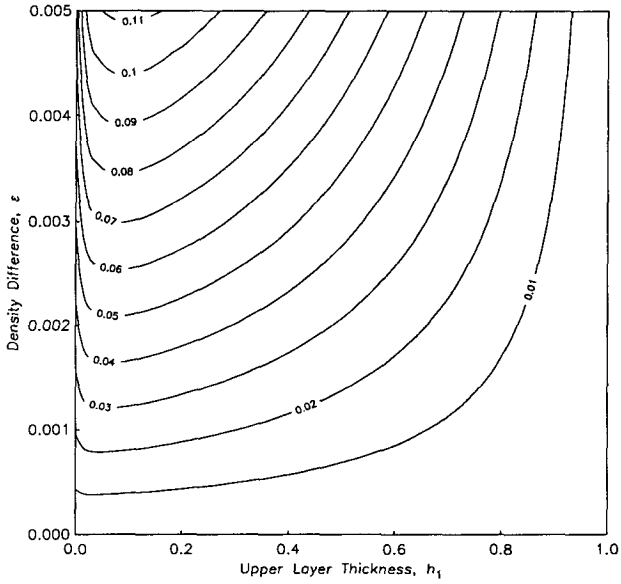

FIG. 4. Contours of the maximum shelf response $|A|_{max}$ for various density differences ϵ and upper-layer thicknesses h_1. Other parameters are $d = 0.0045$, $l = 0$.

the response over the shelf given by (9a) can be simplified to

$$A(\omega) = 2\mu^{-1}/[\cos(\omega/\sqrt{d}) + \lambda i \sin(\omega/\sqrt{d})]$$
$$= \sum_{n=0}^{\infty} Q_n e^{-i\omega(2n+1)/\sqrt{d}} \quad (13)$$

where

$$Q_n = \frac{4\mu^{-1}}{1+\lambda}(-1)^n\left(\frac{1-\lambda}{1+\lambda}\right)^n$$

and λ is independent of ω. Substituting (13) into (12) and using (11) yields

$$\eta^S(x,t) = \frac{1}{2}\sum_{n=0}^{\infty} Q_n\left\{\zeta^P\left[t + \frac{(x+1)}{\sqrt{d}} - \frac{(2n+1)}{\sqrt{d}}\right] + \zeta^P\left[t - \frac{(x+1)}{\sqrt{d}} - \frac{(2n+1)}{\sqrt{d}}\right]\right\} \quad (14a)$$

$$u^S(x,t) = \frac{-1}{2\sqrt{d}}\sum_{n=0}^{\infty} Q_n\left\{\zeta^P\left[t + \frac{(x+1)}{\sqrt{d}} - \frac{(2n+1)}{\sqrt{d}}\right] - \zeta^P\left[t - \frac{(x+1)}{\sqrt{d}} - \frac{(2n+1)}{\sqrt{d}}\right]\right\}. \quad (14b)$$

The shelf response to an incident pulse now becomes fairly clear. The incident pulse generates a surface pulse at the shelf break with amplitude $Q_0/2$ which travels across the shelf toward the coast. It's amplitude doubles to Q_0 at the coast where it reflects from the coastal wall and travels back across the shelf toward the shelf break. Upon reaching the shelf break, part of the pulse is reflected shoreward while part continues into the deep ocean leaking energy to deep-ocean surface and internal waves. This leakage reduces the amplitude of the reflected pulse by the factor $(1-\lambda)/(1+\lambda)$. The reflected part travels toward the coast, repeating the process until the incident energy is entirely gone from the shelf.

To illustrate the shelf response, we consider a single incident pulse with a Gaussian shape and unit amplitude

$$\zeta^P = -e^{-(x+c_-t)^2/\gamma^2} \quad (15)$$

where γ is the pulse half-width (made nondimensional by scaling with the shelf width L) and the negative sign makes the pulse a depression of the interface. We have limited knowledge of the structure of the tidally generated internal wave groups in the Caribbean, so we choose the pulse width to be in the range of those observed in the Sulu Sea (Apel et al. 1985) which were typically 1–4 km wide (γ = 0.05–0.2). Otherwise, the nondimensional quantities appropriate to the Puerto Rico shelf (used in section 3) are chosen here. As in the periodic case, the dimensional response is obtained by multiplying the sea-surface elevation by ζ_i and the velocity by $(g/H)^{1/2}\zeta_i$, where ζ_i is now the dimensional pulse amplitude.

The sea-surface response over the shelf in space and time is shown in Fig. 5 for three different pulse widths. In each case, the pulse maximum arrives at the shelf break at time $t = 0$. The initial shelf pulse can be seen traveling across the shelf and alternately reflecting from the coast and the shelf break. The shelf pulse is clearest for the narrowest incident pulse (γ = 0.05; Fig. 5a). When the pulse width is a greater fraction of the shelf width, then the multiple reflections interfere, and the response closely resembles a lowest mode coastal seiche (Fig. 5c). Another way to view this is that the wider pulse has a narrower Fourier transform, i.e. less energy at the higher frequencies, so the response is smoother in time. Note that the response at the shelf break consists of the initial shelf pulse followed by almost no variations in surface height despite the multiple reflections of the shelf pulse. This suggests that the bottom pressure signal at the shelf break might be a proxy for measuring the incident internal wave signal.

The dynamics of the shelf response are revealed more clearly by the three time series shown in Fig. 6 (all quantities are in nondimensional form). The bottom time series shows the incident pulse arriving at the shelf break at $t = 0$. The uppermost time series is the sea-surface elevation at the coast, while the middle time series is the cross-shelf velocity at the shelf break. There is no response before the pulse arrives. As it arrives, the onshore (negative) velocity in the upper layer above the (negative-amplitude) incident pulse induces an onshore flow at the shelf break. The coastal sea-surface rise is delayed because the information must propagate to the coast at the surface gravity wave speed. Thus, the first maximum sea-surface elevation occurs at t = 15; the nondimensional time required for a gravity wave to cross the shelf, $d^{-1/2}$. After the pulse has reflected from the topography, the sea surface at the coast and the velocity at the shelf break oscillate nearly as a free coastal seiche. The two time series are 90° out of phase with the coastal sea-level maximum occurring when the shelf-break velocity is zero, followed by an offshore flow as the coastal sea level falls. This behavior is also seen clearly in the observations from Puerto Rico (see Giese et al. 1990, Fig. 10).

From the definition of Q_n in (13), the reflection coefficient for the pulse upon encountering the shelf break may be computed exactly. While the full expression is cumbersome, a good approximation can be derived by taking advantage of the fact that $\epsilon \ll 1$. Then, to order $\epsilon^{1/2}$, we obtain

$$\frac{1-\lambda}{1+\lambda} = 1 - 2\sqrt{d} + 3d/2 - (\epsilon/h_1)^{1/2}(2\sqrt{d} - 3d)(1-h_1)^{3/2}. \quad (16)$$

For small d (i.e. a shallow shelf bordering a deep ocean), the value is close to unity meaning that little

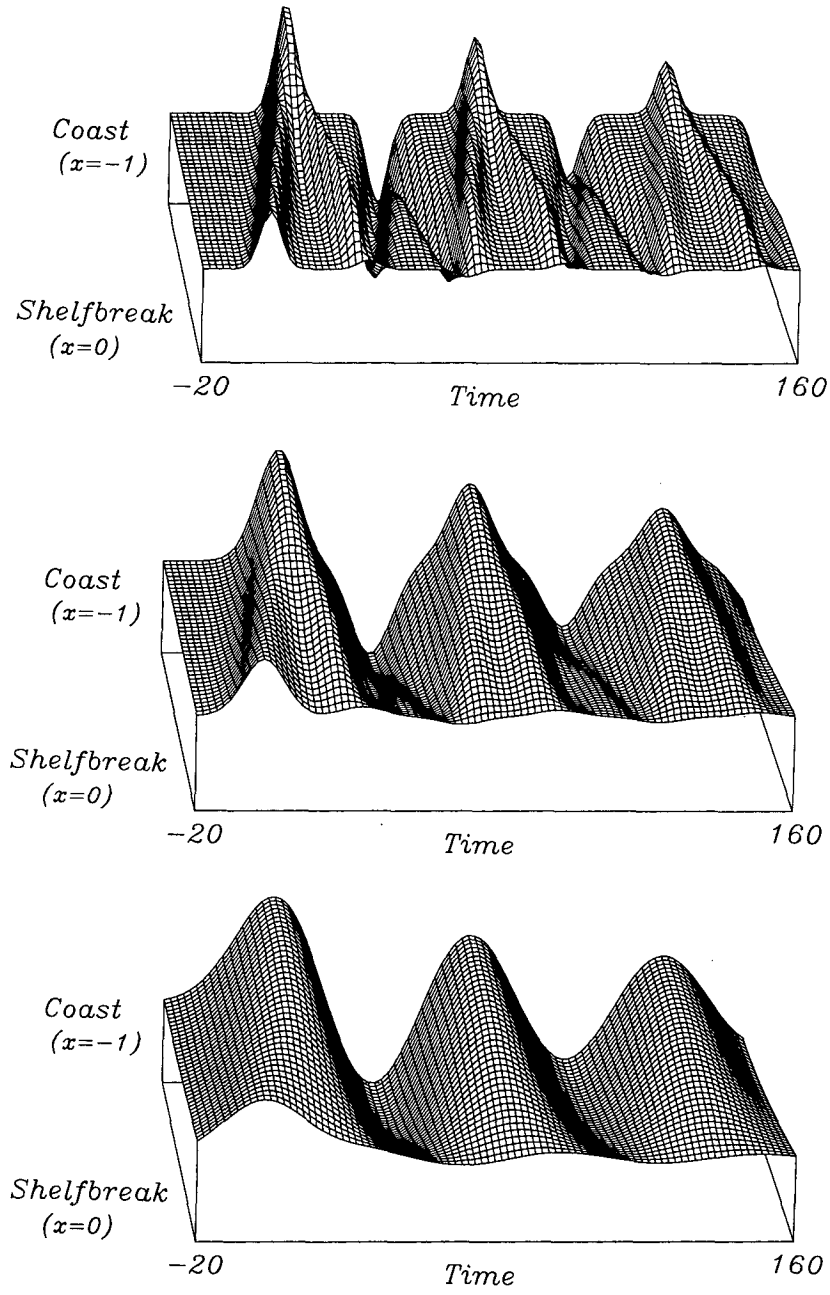

FIG. 5. Sea-surface elevation over the shelf through time in response to a single Gaussian-shaped pulse traveling along the interface normally incident upon the shelf. Pulse width varies with γ = (a) 0.05, (b) 0.1 and (c) 0.2. Other model parameters are $d = 0.0045$, $h_1 = 0.032$, $\epsilon = 0.004$.

energy is lost to the deep sea during the reflection at the shelf break. In this case, the pulse would reflect many times before the shelf energy would be lost. In other words, the seiching would continue long after the arrival of the pulse. The shelf break reflection coefficient corresponding to the case in Fig. 6 is 0.835, and the ringing is obvious. Notice that the reflection coefficient decreases with increasing stratification. This occurs because the deep-ocean internal waves are more efficiently excited when the stratification is stronger. So, although the initial response is larger when the stratification is stronger, the resultant seiching will decay more rapidly after the forcing ceases.

The magnitude of the shelf response to the single pulse is much smaller than that of the peaks in Fig. 3 because the pulse contains less energy at the lowest-

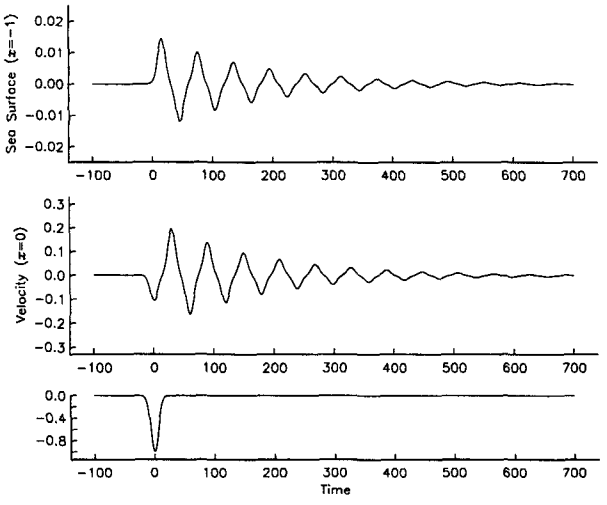

FIG. 6. Time series of (upper) sea surface elevation at the coast and (middle) cross-shelf velocity at the shelf break, which result from an incident pulse whose interface displacement at the shelf break is shown in the lower time series. For this case, $d = 0.0045$, $h_1 = 0.032$, $\epsilon = 0.004$, $\gamma = 0.1$.

mode seiche frequency. In dimensional units, if the incident pulse amplitude is 10 m (actually rather small based on the Sulu Sea observations of Apel et al. 1985), then a nondimensional sea-surface displacement of 0.01 corresponds to about 10 cm, while a nondimensional velocity of 0.10 corresponds to about 5 cm s^{-1}. Thus the magnitudes of the responses shown in Fig. 6 (maximum coastal sea level of 14 cm; maximum shelf-break velocity of 10 cm s^{-1}) are both similar to those observed off Puerto Rico during strong seiches (Giese et al., 1990).

The beauty of the solution (14) is that the shape of the incident signal is arbitrary (providing it is bounded), so various forms of forcing can be considered easily. For example, Fig. 7 shows the response to two pulses, each of which is identical to the pulse in Fig. 6, and separated by $\Delta t = 60$ nondimensional time units. This Δt is nearly equal to the period of the lowest-mode seiche oscillation and results in an amplified (resonant) response. Note that the scales in Fig. 7 are the same as those in Fig. 6, so a pair of 10 m pulses generates sea-surface displacements at the coast which reach 20 cm and cross-shelf velocities at the shelf break which reach 15 cm s^{-1}. On the other hand, if the two pulses are separated by $\Delta t = 80$ units, then the response (Fig. 8) is about the same size as that for a single pulse (Fig. 6). Figure 8 also shows that, while the dominant response is at the seiche frequency, the pattern of shelf oscillations is generally irregular with the details depending on the number, size and time delay between pulses.

5. Discussion

The model presented here is intended to demonstrate a dynamical mechanism by which baroclinic energy in the form of deep-sea internal waves can be transferred to barotropic coastal seiches. At this point, the results should be interpreted primarily qualitatively because of the simplifying assumptions made in the model formulation. The most important of these are discussed here. First, the linearity of the model technically restricts the discussion to small-amplitude waves, so large pulses like those observed in the Sulu Sea (Apel et al. 1985) cannot strictly be considered. As a result, the linear phase speed is slightly less than that of the internal solitary waves, so that the time during which a solitary wave interacts with the topography would probably appear somewhat shorter than in the linear case. However, this may effectively introduce more en-

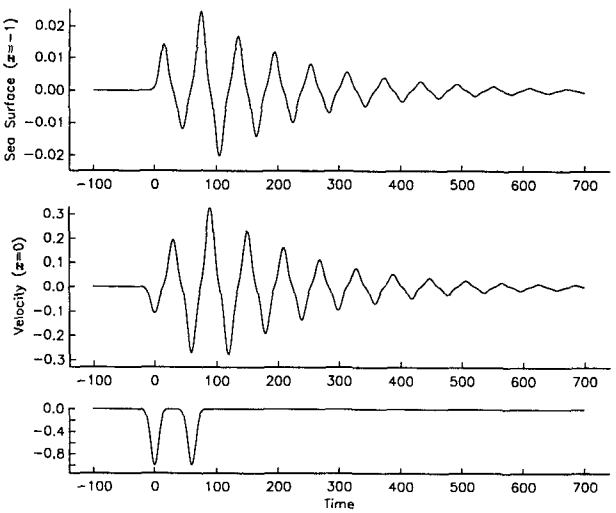

FIG. 7. As in Fig. 6 but for two incident pulses, each with $\gamma = 0.1$, and separated by $\Delta t = 60$ nondimensional time units.

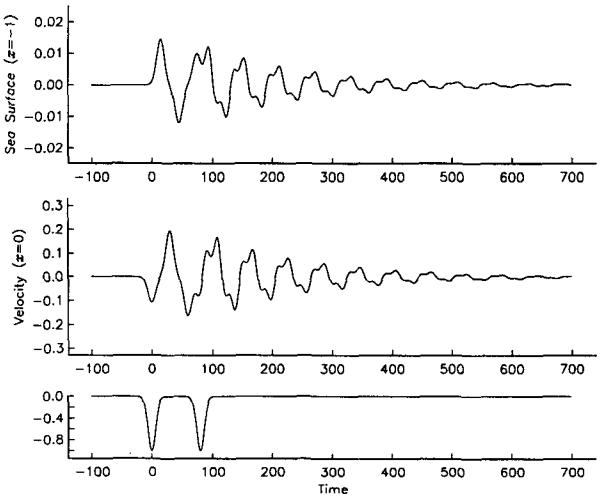

FIG. 8. As in Fig. 7 but the two pulses are separated by $\Delta t = 80$ time units.

ergy at the higher frequencies than is present in a linear pulse which would increase the seiche response.

The use of the shallow-water approximation in the deep ocean (as discussed in the Appendix) is another model limitation. It certainly is violated by the very high frequency components of the solution (12) which would lead to some dispersive effects. However, the approximation is quite good near the seiche frequency and there is so little energy at the very high frequencies that the errors are negligible. Furthermore, any dispersive effects would be unimportant for the short time during the actual interaction of the pulse with the topography.

Another limitation is the simple stratification used here. We have shown that the model is sensitive to the degree of stratification, but more realistic stratification should be included to model the detailed energy transfer more accurately. One step toward a more realistic representation of the stratification is to allow continuous stratification in the lower layer. Such an extension of the present model is the subject of a forthcoming paper by Grimshaw and Chapman.

Perhaps the most serious limitation is introduced by the simple topography. In the present model, all of the incident energy is reflected back to the deep ocean. On the other hand, internal solitary waves impinging on a sloping bottom would surely steepen and break, creating mixing and turbulence and altering the transfer of baroclinic energy to the seiches. To study these processes, realistic bottom topography and more complex dynamics must be included in the model. We leave this for the future.

One feature which has been neglected, but which can be shown to have little effect, is bottom friction over the shelf. As in Chapman (1984), bottom friction can be added in the form of the terms $-ru$ and $-rv$ on the right-hand sides of (1a) and (1b), respectively, when applied to the shelf. Here r is the bottom friction coefficient which is scaled by $(gH)^{1/2}/L$. The only change in (5)–(9) and (12) is that d is everywhere replaced by d/F, where $F = 1 - ir/\omega$. (Now $\alpha^2 = \omega^2 F/d - l^2$.) However, $A(\omega)$ can no longer be written as in (13), so (12) must be evaluated numerically. This has been done for the case equivalent to that shown in Fig. 6 with $r = 0.003$. In dimensional units, this friction coefficient has the (rather large) value of 0.11 cm s^{-1} for an 18 m deep shelf. Results show that the amplitudes of the first few oscillations in Fig. 6 are almost unchanged (not shown). The primary effect is that the frictional response decays slightly faster.

6. Conclusion

The model results presented here suggest that deep-sea internal waves can generate coastal seiches of significant amplitude. The most important factors required appear to be large-amplitude internal waves (e.g. tidally generated solitary waves) and strong vertical stratification. These results provide a dynamical mechanism for the transfer of baroclinic energy to barotropic coastal seiches in general, and specifically provide an explanation for the observed seiche activity along the Caribbean coast of Puerto Rico. The lowest-mode seiche tends to be the most highly excited, and substantial sea-level oscillations at the coast with large currents at the shelf break are predicted. A truly quantitative comparison with observations will require a more sophisticated model as well as a more complete data set.

Acknowledgments. Several perceptive comments from Rob Pinkel, Nelson Hogg, Karl Helfrich and Steve Lentz proved quite helpful and are much appreciated. We are particularly grateful to Roger Grimshaw for showing us how to evaluate the Fourier integral solution (12) analytically. During the course of this research, support was provided by the National Science Foundation under Grants OCE85-21837 and OCE90-23065, by an Independent Study Award from the Woods Hole Oceanographic Institution, and by the Institution's Coastal Research Center.

APPENDIX

Justification for the Shallow-Water Approximation

The shallow-water approximation is a key assumption in the present model because it removes all dispersive effects (i.e. all wavelengths of internal waves have the same phase speed) which allows the construction of a coherent wave pulse by superposition of periodic solutions. However, because the deep ocean depth is 4000 m and the seiche period (50 min) is fairly short, the approximation should be explicitly justified.

The most stringent test of the approximation is to compare the wavelengths and phase speeds of the internal waves with and without making the shallow-water approximation because the internal waves are shorter than the surface waves at any given frequency, and hence, will be affected more by the assumption of shallow water. The comparison is made here for unidirectional waves over a flat bottom. All variables are dimensional in this Appendix.

In the nonshallow water case, the wave solutions are found by solving the irrotational, two-layer problem as follows. A velocity potential in introduced as $(u, v, w) = \nabla\phi$ which leads to Laplace's equation for each layer:

$$\nabla^2\phi^U = 0; \quad \nabla^2\phi^L = 0. \tag{17}$$

The pressure is set to zero at the upper surface

$$\phi_{tt}^U + g\phi_z^U = 0 \quad \text{at} \quad z = 0 \tag{18}$$

while the vertical velocity and pressure must match at the interface

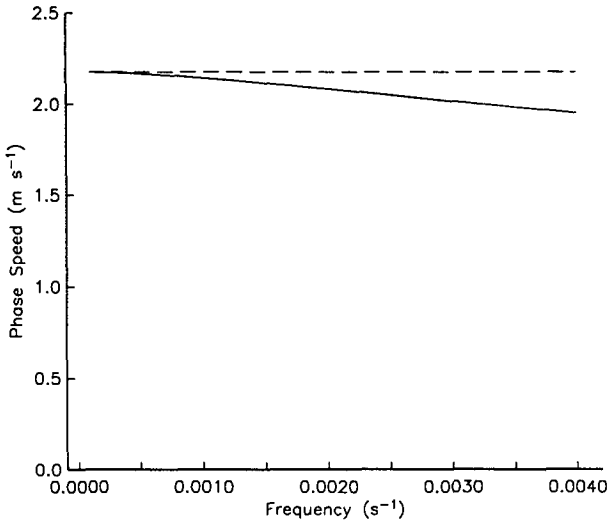

FIG. A1. Phase speed versus frequency for the exact linear model (i.e. without making the shallow-water approximation; solid curve) and the shallow water model (dashed curve). The seiche frequency at Puerto Rico is 0.002 s^{-1}. Dimensional parameters for this plot are $h_1 = 128$ m, $H = 4000$ m, $\rho^U = 1.024$ g cm^{-3}, $\rho^L = 1.028$ g cm^{-3}.

$$\phi_z{}^U = \phi_z{}^L \quad \text{at} \quad z = -h_1 \tag{19}$$

$$\rho^U(\phi_{tt}^U + g\phi_z{}^U) = \rho^L(\phi_{tt}^L + g\phi_z{}^L) \quad \text{at} \quad z = -h_1 \tag{20}$$

where ρ^U, ρ^L are the upper and lower layer densities, respectively. Finally, the vertical velocity must vanish at the flat bottom

$$\phi_z{}^L = 0 \quad \text{at} \quad z = -H. \tag{21}$$

Assuming a periodic free wave solution with time and space dependence of $\exp(-i\sigma + i\beta x)$, then equation (17), along with the boundary and matching conditions (18)–(21), can be reduced to a single dispersion relation of the form

$$\rho^U \tanh(\beta h_1)(\sigma^4 - g^2\beta^2) + \rho^L[\sigma^2 - g\beta \tanh(\beta h_1)] \times [\sigma^2 \coth(\beta h_2) - g\beta] = 0 \tag{22}$$

which relates the wavenumber β and frequency σ. The phase speed is then $c = \sigma/\beta$.

The equivalent phase speed and wavenumber for the shallow water case are given by (3) with $l = 0$. Using dimensional variables, these become

$$c_{sw}{}^2 = \frac{1}{2} gH\left[1 - \left(1 - \frac{4\epsilon h_1 h_2}{H^2}\right)^{1/2}\right] \tag{23}$$

$$\beta_{s\omega} = \sigma/c_{s\omega}. \tag{24}$$

The parameters appropriate for the Caribbean Sea just offshore of Puerto Rico are $h_1 = 128$ m, $H = 4000$ m, $\rho^U = 1.024$ g cm^{-3}, $\rho^L = 1.028$ g cm^{-3} and $g = 9.8$ cm s^{-2}. Using these values, the 'exact' linear phase speed can be computed from (22) for a variety of frequencies. (Of course, $c_{s\omega}$ is independent of frequency.) Figure A1 shows that the shallow water phase speed is quite close to the exact linear phase speed (within 12%) up to a frequency of 0.004 s^{-1}. This is twice the seiche frequency of 0.002 s^{-1} indicating that the shallow-water approximation is quite good in this situation. The reason is that, although the deep-ocean depth is comparable to the wavelength of the internal wave at the seiche frequency (6540 m), the upper layer is still very thin in comparison.

REFERENCES

Apel, J. R., J. R. Holbrook, A. K. Liu and J. J. Tsai, 1985: The Sulu Sea internal soliton experiment. *J. Phys. Oceanogr.*, **15**, 1625–1651.

Chapman, D. C., 1984: The generation of barotropic edge waves by deep-sea internal waves. *J. Phys. Oceanogr.*, **14**, 1152–1158.

Froelich, P. N., D. K. Atwood and G. S. Giese, 1978: Influence of Amazon River discharge on surface salinity and dissolved silicate concentration in the Caribbean Sea. *Deep-Sea Res.*, **25**, 735–744.

Giese, G. S., and R. B. Hollander, 1987: The relationship between coastal seiches at Palawan Island and tide-generated internal waves in the Sulu Sea. *J. Geophys. Res.*, **92**, 5151–5156.

——, ——, J. E. Fancher and B. S. Giese, 1982: Evidence of coastal seiche excitation by tide-generated internal solitary waves. *Geophys. Res. Lett.*, **9**, 1305–1308.

——, D. C. Chapman, P. G. Black and J. A. Fornshell, 1990: Causation of large-amplitude coastal seiches on the Caribbean coast of Puerto Rico, *J. Phys. Oceanogr.*, **20**, 1449–1458.